

Article

Evaluation of Corrosion Behavior on Crept AlSi10MnMg (AA365) Alloy Produced by High-Pressure Die-Casting (HPDC)

Seonghwan Park, Cheolmin Ahn and Eunkyung Lee *

Interdisciplinary Major of Maritime AI Convergence, Department of Ocean Advanced Materials Convergence Engineering, Korea Maritime and Ocean University, Busan 49112, Korea; tjdghks784@naver.com (S.P.); asdf151512@naver.com (C.A.)

* Correspondence: elee@kmou.ac.kr; Tel.: +82-(051)-410-4353

Abstract: High-pressure die-cast AlSi10MnMg (AA365) alloys have been used as a material for automotive components exposed to high temperature and corrosive environments. This work determines the correlation of corrosion resistance with the intermetallic compounds and micro-voids of crept AA365 alloys under temperatures ranging from 373 K to 573 K with various applied stresses. The results showed that crept AA365 alloy at 473 K possessed a large amount of the intermetallic phases, compared with crept AA365 alloys at 373 K and 573 K due to the non-equilibrium solute atoms in Al matrix. By contrast, crept AA365 alloy at 573 K contained the lowest number of intermetallic precipitates owing to the remelting of the phases. With regard to the corrosion behavior, the corrosion potentials showed -687.0 , -684.0 , and -673.0 mV_{SCE} of crept AA365 alloys at 373 K, 473 K, and 573 K, respectively, which means the corrosion occurred slowly on the crept AA365 alloy at 573 K, rather than at 373 K, 473 K. The value of the corrosion current density (I_{corr}) in the crept HPDC AA365 alloy at 473 K has the highest corrosion current density of 13.3×10^{-6} Acm⁻², compared with others. It can be inferred that the high amount of intermetallic compounds gave rise to severe corrosion and led to the harmful micro-galvanic corrosion of crept AA365 alloy, rather than the micro-voids.



Citation: Park, S.; Ahn, C.; Lee, E. Evaluation of Corrosion Behavior on Crept AlSi10MnMg (AA365) Alloy Produced by High-Pressure Die-Casting (HPDC). *Appl. Sci.* **2021**, *11*, 6227. <https://doi.org/10.3390/app11136227>

Academic Editor: Karl Ulrich Kainer

Received: 10 May 2021

Accepted: 29 June 2021

Published: 5 July 2021

Publisher's Note: MDPI stays neutral with regard to jurisdictional claims in published maps and institutional affiliations.



Copyright: © 2021 by the authors. Licensee MDPI, Basel, Switzerland. This article is an open access article distributed under the terms and conditions of the Creative Commons Attribution (CC BY) license (<https://creativecommons.org/licenses/by/4.0/>).

Keywords: aluminum alloy; corrosion; microstructure; temperature; intermetallic compounds

1. Introduction

Due to problems with the regulation of environments and fuel efficiency, it is necessarily required to use lightweight materials in various industries, such as automotive, marine, and aerospace fields. Under such circumstances, aluminum alloy has been given attention by many industries owing to the significant advantages of lighter weight, excellent corrosion resistance, and high-strength stiffness to weight ratio [1]. In particular, AlSi10MnMg (Silafont-36, AA365) alloy is the first successful aluminum–silicon alloy of low iron content and has many benefits, such as good castability, excellent wear, and corrosion resistance, and high elongation [2]. Moreover, this alloy has been primarily produced by the high-pressure die-casting (HPDC) process, which has contributed to high productivity and capability to produce complicated components [3,4]. With such advantages, the HPDC AA365 alloy has been employed extensively as automotive components, notably powertrain systems in automobiles, such as a cylinder head, engine block, and engine room parts [2]. However, the components adjacent to the engine are exposed to high-temperature and corrosive environments. So, these parts should be required for excellent corrosive resistance and high-temperature mechanical property. In addition, the HPDC process can give rise to many defects, such as micro-voids and trapped gas, and the defects can provoke the inferior performance of the alloy parts by propagating cracks [2,5–7].

In terms of the microstructure of Al–Si alloy, α -Al phase, hard Si phase, and brittle intermetallic phases are usually found. In this, intermetallic phases are laid mainly as β -Al₅SiFe, α -Al₁₅(Mn,Fe)₃Si₂, Mg₂Si, and π -Al₈Mg₃FeSi₆ [8–10]. In the corrosive environment, the Si particle and intermetallic phases react as local cathodes with respect to the

α -Al phase, generating localized corrosion through the eutectic areas [7]. In other words, they can lead to the formation of micro-galvanic couples, degrading the performance of the Al alloy. However, the effect of the Si particles would be insignificant because of the low current density, as a result of the high polarization of the particles comparatively [7]. Instead, the intermetallic compounds may lead to intense galvanic couples with the α -Al matrix, showing severe pitting corrosion on the parts.

Previous research has investigated the various characteristics of AlSi10MnMg alloys. In terms of the microstructure, casting defects, heat treatment, mechanical properties, and corrosion resistance of the alloy have been examined [11–14]. Furthermore, it was found that the characteristics have been varied, depending on the cooling rates of AlSi10MnMg alloy after T4 (solidification + solid solution treatment) and T6 heat treatments (solidification + solid solution treatment + artificial aging) [9]. Especially, the superior creep resistance of the alloy has been proved under the various high-temperature and applied stresses, of which this ability was attributed to the threshold stress which stemmed from the interaction of dislocations and intermetallic compounds [2]. However, few studies have been conducted about the corrosion properties of an AlSi10MnMg alloy affected by applied stress under high temperature.

The purpose of this research was to investigate the corrosion behavior of crept AlSi10MnMg alloy (AA365) from the point of microstructural view, in order to contribute to improving the reliability and long-term structural performance of this application in the automotive industry. To examine this characteristic of the alloys, this study revealed the correlation between the corrosion resistance and the microstructures, notably intermetallic compounds and micro-voids, of crept AA365 alloys affected by various temperatures and stresses. Such results would be helpful to understand the relationship between the microstructures subjected to the long-term temperature with applied stresses and the corrosion characteristic.

2. Materials and Methods

A sample of AA365 (Silafont 36) alloy produced by high-pressure die-casting (HPDC) was supplied by Rio Tinto (USA). Spectrometry analysis (SpectroMaxX Spark, Spectro, Germany) was utilized to measure the elemental composition, as shown in Table 1 [2].

Table 1. Chemical composition of AA365 aluminum alloy.

	Si	Mn	Mg	Fe	Ti	Al
AA365	10.6	0.7	0.28	0.1	0.08	Bal.

Cylindrical creep specimens of HPDC AA365 alloy with 12mm in diameter and 27mm in a gauge length were machined. Then, a creep-testing machine (UL200N–1603144) was used for the creep test in accordance with ASTM E319. Detailed information can be found in the preliminary experiment [2]. Three crept samples, i.e., crept AA365 alloy at 373 K with the applied stress of 190 MPa, crept AA365 alloy at 473 K with the applied stress of 120 MPa, crept AA365 alloy at 573 K with the applied stress of 80 MPa, were selected for corrosion test because many intermetallic compounds were formed and re-dissolved under these conditions. For corrosion tests of three crept samples, a computer-controlled GAMRY potentiostat (Interface 1010E Potentiostat, Gamry Instruments, Warminster, PA, USA) and a three-electrode electrochemical cell system, where a saturated calomel electrode (SCE) was carried out with a saturated calomel electrode (SCE) as a reference electrode (RE), a platinum plate as a counter electrode (CE), and a test sample used as a working electrode (WE). Then, 3.5 wt% sodium chloride (NaCl) was used for the corrosion tests. Three crept AA365 alloys were polished with SiC polishing paper up to grit 2400, a 0.25 μ m diamond suspension, and a 0.04 μ m colloidal suspension consecutively for a reduction in the effect of micro-scratch on the corrosion properties of the alloy. All the tests were performed at room temperature. Before the electrochemical testing, open circuit potential (OCP) was measured

for 1 h to stabilize the crept AA365 alloys. Then cyclic potentiodynamic polarization (CPDP) was conducted from an initial potential of -500 mV to the final potential of $+1100$ mV with a scanning rate of 0.1 mV/s and limiting the current to 10 mA/cm². In trying to evaluate the data, Gamry Echem Analyst software was used. The cyclic potentiodynamic polarization curves were plotted with corrosion rate, corrosion current density, and corrosion potential measured by the Tafel extrapolation method.

Crept AA365 samples were cut by a cutting machine and polished in order of silicon carbide (SiC) polishing paper up to grit 2400, a 0.25 μm diamond suspension, and 0.04 μm colloidal suspension. Following polishing, a field emission scanning electron microscope (FE-SEM; MIRA3, Tescan) with an energy-dispersive X-ray spectroscopy (EDS, EDAX) module was carried out with an accelerating voltage of 15 kV in attempting to investigate the microstructure of crept AA365 specimens. For analyzing chemical elements of intermetallic phases distributed in the Al matrix, an electron probe X-ray microanalyzer (EPMA, JXA-8230, JEOL) was used.

3. Results and Discussion

3.1. Microstructure of Crept HPDC AA365 Alloy

The microstructure of crept AA365 alloys at various temperatures was shown in Figure 1. In terms of voids, as temperature increased, the presence of porosities raised relatively. This is because, with the increase in temperature, micro-voids were diffused, growing the size of the voids up [2]. When it comes to the density of the intermetallic compounds, crept AA365 alloy at 473 K shown in Figure 1b has a large amount of the intermetallic phases [15]. Before the creep test, rapid solidification caused by the HPDC process led to the non-equilibrium solute elements in the Al matrix, meaning that the supersaturated α -Al was thermodynamically unstable. Therefore, upon the temperature applied during the creep test, the excessive content of the elements expelled out of the Al matrix to form the intermetallic compounds. This behavior explains why the density of the intermetallic precipitates in crept AA365 alloy at 473 K was relatively higher than other alloys. On the other hand, crept AA365 alloy at 573 K contained the lowest density of the secondary phases, as seen in Figure 1c. This was attributed to the fact that the intermetallic compounds were re-dissolved into the Al matrix at 573 K, generating the decrement in the secondary phases. The EDS analysis results showed that the brittle intermetallic compounds on the Al matrix of the crept AA365 alloys were identified as π -Al₁₂FeMg_{1.5}Si₅ and α -Al₁₆(Mn,Fe)Si₃, as shown in Figure 1d [16].

EPMA analysis, shown in Figure 2, revealed that the brittle intermetallic compounds on the Al matrix were identified as π -AlFeMgSi and α -AlMnFeSi phases, resulting in less detrimental effects on mechanical properties. These intermetallic precipitates were observed at the boundaries of α -Al grain because grain boundaries having higher energy than intergranular grain facilitated the production of the intermetallic compounds at the boundaries.

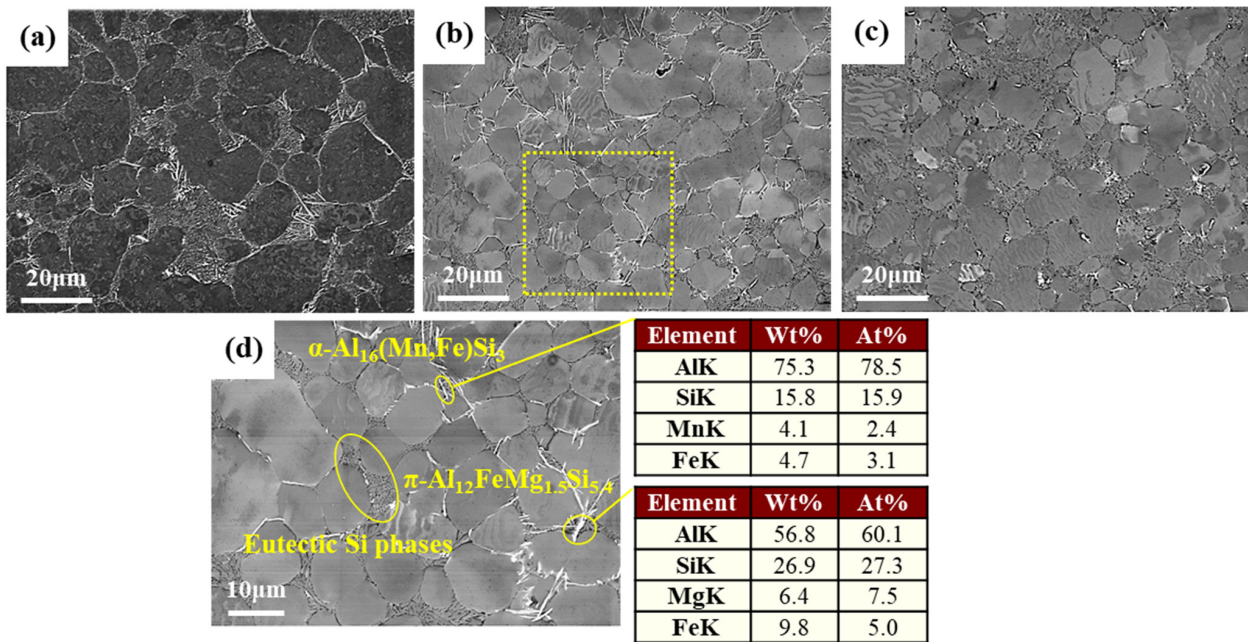


Figure 1. SEM and EDS analysis of microstructure of crept HPDC AA365 alloys: (a) crept AA365 alloy at 373 K; (b) crept AA365 alloy at 473 K; (c) crept AA365 alloy at 573 K; (d) A higher magnification micrograph and EDS analysis of crept AA365 alloy at 473 K.

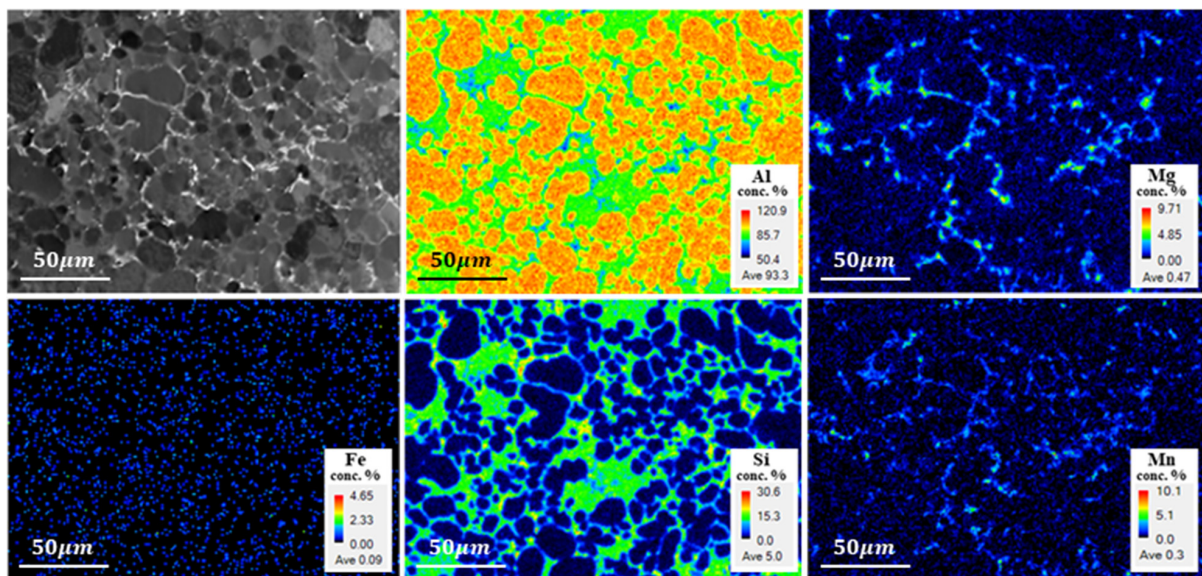


Figure 2. EPMA micrograph and chemical element distribution maps of crept AA365 alloy at 373 K: Al, Mg, Fe, Si, Mn.

3.2. Electrochemical Characteristic of Crept HPDC AA365 Alloy

Figure 3 showed the variation of the open circuit potential (OCP) of the crept AA365 alloys at various temperatures as a function of immersion time in 3.5% wt.% NaCl. It can be shown that continuous fluctuations were found in all samples during an hour of immersion. This would imply that passivation film on the surface would be removed with the chemical reaction in the solution at first. However, the surface would be covered with an oxide film by reacting to the solution later. This phenomenon explained why continuous fluctuations were observed [17]. The corrosion characteristics of crept AA365 alloys were indicated after the cyclic potentiodynamic polarization in 3.5 wt.% NaCl, according to

Figure 4. The corrosion potential (E_{corr}) and the corrosion current density (I_{corr}) were calculated by using Tafel extrapolation from these curves, and the values of these results were listed in Table 2. All crept HPDC AA365 alloys showed that the corrosion potentials were comparable to the pitting potential (E_{pit}) with the rapid increase in current density on the anodic branch. Few passivation behaviors were observed in the anodic branch, and the trend of all AA365 alloys brought the pitting attack without any limitations at the corrosion potential. Moreover, the corrosion potentials indicated -687 , -684 , and -673 mV_{SCE} of crept AA365 alloys at 373 K, 473 K, and 573 K, respectively. It meant that the corrosion occurred rapidly on the crept AA365 alloy at 473 K rather than other alloys. Above the pitting potential, new pits on the matrix were expected to nucleate, grow, and propagate, causing the pitting corrosion on the crept alloy. After reversing the scan in these curves, the pit's growth declines incrementally until reaching the repassivation potential. Especially, the corrosion current density (I_{corr}) was investigated to evaluate the corrosion resistance of the alloys in general. The values of I_{corr} were determined as 8.02 , 13.3 , and 0.51×10^{-6} Acm⁻², respectively. The crept HPDC AA365 alloy at 473 K showed the highest corrosion current density, rather than others. It could be argued that the high amount of intermetallic compounds led the crept alloy at 473 K to severe corrosion, as proved in Figure 4. In attempting to understand the corrosion attack on the crept HPDC AA365 alloys after the electrochemical test in 3.5 wt.% NaCl, the corroded surface morphology of these alloys was exhibited in Figure 5. As expected about the micro-galvanic corrosion between the intermetallic precipitates and the Al matrix, the localized corrosion on the Al matrix in the vicinity of the intermetallic compounds was formed owing to the high potential difference between the Al matrix and the intermetallic compounds. Especially, the corrosion of crept HPDC AA365 alloy at 473 K severely occurred owing to the highest density of the intermetallic precipitates. Based on the results, it can be concluded that the intermetallic compounds on the Al matrix gave rise to the harmful micro-galvanic corrosion of crept HPDC AA365 alloys rather than the point defects, such as micro-voids, shrinkages, and trapped gas.

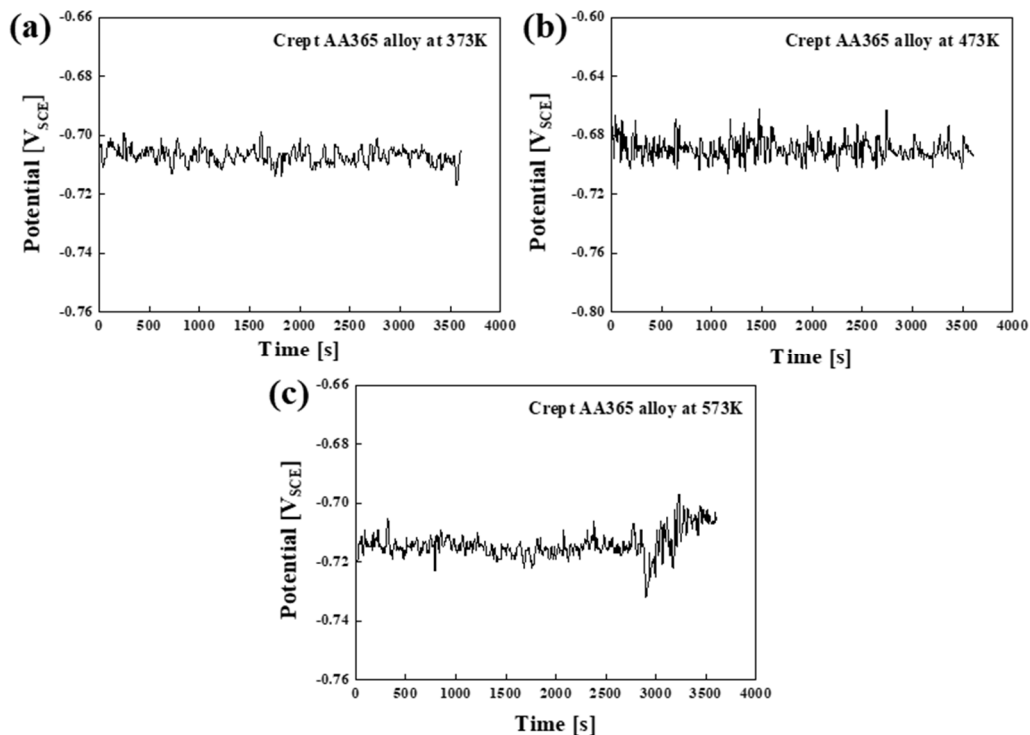


Figure 3. Variation of the open circuit potential (OCP) of crept AA365 alloys in 3.5 wt.% NaCl during a hour of immersion: (a) crept AA365 alloy at 373 K; (b) crept AA365 alloy at 473 K; (c) crept AA365 alloy at 573 K.

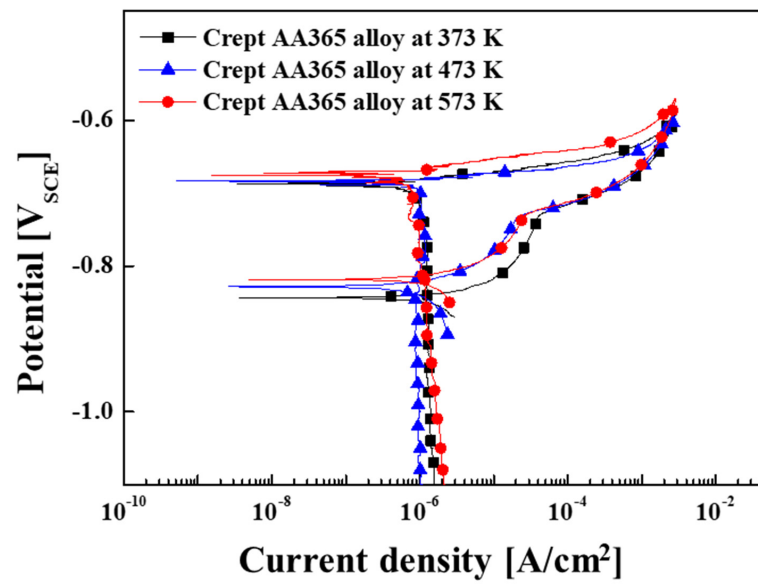


Figure 4. Cyclic potentiodynamic polarization (CPDP) curves of crept HPDC AA365 alloys in 3.5 wt.% NaCl.

Table 2. Cyclic potentiodynamic polarization parameters obtained for crept HPDC AA365 alloys in 3.5 wt.% NaCl.

Condition		E_{corr} (mV)	I_{corr} ($\times 10^{-6} \text{ A cm}^{-2}$)	Anodic Slope (mV/dec)	Cathodic Slope (mV/dec)
AlSi10MnMg (AA365) alloy	373 K	−687	8.02	19.5	49.1
	473 K	−684	13.3	6.6	39.9
	573 K	−673	0.51	8.9	18.8

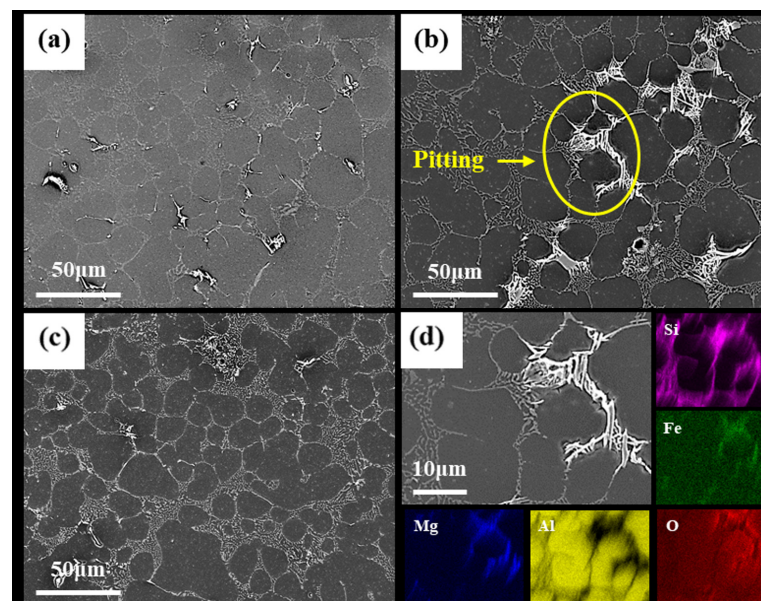


Figure 5. SEM and EDS analysis of corroded surface morphology of crept HPDC AA365 alloys of the attack after electrochemical testing in 3.5 wt.% NaCl: (a) crept HPDC AA365 alloy at 373 K; (b) crept HPDC AA365 alloy at 473 K; (c) crept HPDC AA365 alloy at 573 K; (d) BSE image of crept HPDC AA365 alloy at 473K along with the EDS elemental maps of Al, Si, Fe, Mg, and O.

4. Conclusions

This work was carried out to understand the correlation the corrosion resistance with the microstructure, intermetallic compounds, and micro-voids of crept HPDC AA365 alloys affected by various temperatures and stresses. The conclusions are as mentioned below.

- 1 In all crept AA365 alloys, intermetallic precipitates were located at α -Al grain boundaries due to the fact that grain boundaries have higher energy than intergranular grain, promoting the production of intermetallic compounds at the boundaries. With regard to voids, as the temperature increased, the presence of porosities raised comparatively, owing to the diffusion of micro-voids. In terms of the density of the intermetallic phases, crept AA365 alloy at 473 K has a large amount of the secondary phases in comparison with crept AA365 alloys at 373 K and 573 K. The unstable supersaturated α -Al accounted for the highest density of the intermetallic compounds in crept AA365 alloy at 473 K. By contrast, crept AA365 alloy at 573 K possessed the lowest density of the intermetallic precipitates because of the re-dissolution of the phases at 573 K occurred.
- 2 The corrosion characteristics of all crept AA365 alloys showed that the corrosion potentials were similar to the pitting potential (E_{pit}) with the rapid increase in current density on the anodic branch. Furthermore, the corrosion potentials exhibited -687 , -684 , and -673 mV_{SCE} of crept AA365 alloys at 373 K, 473 K, and 573 K, respectively, implying that the corrosion happened quickly on the crept AA365 alloy at 473 K rather than at 373 K or 573 K. The value of the corrosion current density (I_{corr}) in the crept HPDC AA365 alloy at 473 K has the highest corrosion current density of 13.3×10^{-6} Acm⁻², compared with other alloys.
- 3 It can be deduced that the high amount of intermetallic compounds gave rise to the severe corrosive effect and led to the harmful micro-galvanic corrosion of crept HPDC AA365 alloy rather than the point defects, including micro-voids, shrinkages, and trapped gas.

The current research found the relationship between the corrosion and the microstructure, involving intermetallic compounds and micro-voids of crept HPDC AA365 aluminum alloy at temperatures ranging from 373 K to 573 K with various stresses. The consequences would help to guarantee the reliability and long-term structural performance of this application in the automobile industry.

Author Contributions: Conceptualization, S.P., C.A. and E.L.; validation, S.P., C.A. and E.L.; formal analysis, S.P., C.A. and E.L.; investigation, S.P., C.A. and E.L.; data curation, S.P. and C.A.; methodology, S.P. and C.A.; visualization, S.P. and C.A.; resources, S.P. and C.A.; writing—original draft preparation, S.P. and C.A.; supervision, E.L.; project administration, E.L.; funding acquisition, E.L.; writing—review and editing, E.L. All authors have read and agreed to the published version of the manuscript.

Funding: This research was supported by the National Research Foundation of Korea (NRF) granted by the Korean Government (NRF-2019R111A3A01062863).

Institutional Review Board Statement: Not applicable.

Informed Consent Statement: Not applicable.

Data Availability Statement: The data presented in this study are available on request from the corresponding author.

Conflicts of Interest: The authors declare no conflict of interest.

References

1. Dias, M.; Oliveira, R.; Kakitani, R.; Cheung, N.; Henein, H.; Spinelli, J.E.; Garcia, A. Effects of solidification thermal parameters and Bi doping on silicon size, morphology and mechanical properties of Al-15wt.% Si-3.2wt.% Bi and Al-18wt.% Si-3.2wt.% Bi alloys. *J. Mater. Res. Technol.* **2020**, *9*, 3460–3470. [[CrossRef](#)]

2. Ahn, C.; Jo, I.; Ji, C.; Cho, S.; Mishra, B.; Lee, E. Creep behavior of high-pressure die-cast AlSi10MnMg aluminum alloy. *Mater. Charact.* **2020**, *167*, 110495. [[CrossRef](#)]
3. Jaglinski, T.; Lakes, R. Creep Behavior of Al-Si Die-Cast Alloys. *J. Eng. Mater. Technol.* **2004**, *126*, 378–383. [[CrossRef](#)]
4. Sadeghi, M.; Mahmoudi, J. Experimental and Theoretical Studies on the Effect of Die Temperature on the Quality of the Products in High-Pressure Die-Casting Process. *Adv. Mater. Sci. Eng.* **2012**, *2012*, 1–9. [[CrossRef](#)]
5. Avalle, M. Casting defects and fatigue strength of a die cast aluminium alloy: A comparison between standard specimens and production components. *Int. J. Fatigue* **2002**, *24*, 1–9. [[CrossRef](#)]
6. Zhang, B.; Cockcroft, S.L.; Maijer, D.M.; Zhu, J.D.; Phillion, A. Casting defects in low-pressure die-cast aluminum alloy wheels. *JOM* **2005**, *57*, 36–43. [[CrossRef](#)]
7. Qi, M.; Kang, Y.; Qiu, Q.; Tang, W.; Li, J.; Li, B. Microstructures, mechanical properties, and corrosion behavior of novel high-thermal-conductivity hypoeutectic Al-Si alloys prepared by rheological high pressure die-casting and high pressure die-casting. *J. Alloy. Compd.* **2018**, *749*, 487–502. [[CrossRef](#)]
8. Lee, E.; Mishra, B. Effect of Solidification Cooling Rate on Mechanical Properties and Microstructure of Al-Si-Mn-Mg Alloy. *Mater. Trans.* **2017**, *58*, 1624–1627. [[CrossRef](#)]
9. Lee, E.; Mishra, B. Effect of Cooling Rate on the Mechanical Properties of AA365 Aluminum Alloy Heat-Treated Under T4, T5, and T6 Conditions. *Int. J. Met.* **2017**, *12*, 449–456. [[CrossRef](#)]
10. Narayanan, L.A.; Samuel, F.H.; Gruzleski, J.E. Crystallization behavior of iron-containing intermetallic compounds in 319 aluminum alloy. *Met. Mater. Trans. A* **1994**, *25*, 1761–1773. [[CrossRef](#)]
11. Niklas, A.; Bakedano, A.; Orden, S.; da Silva, M.; Nogués, E.; Fernández-Calvo, A.I. *Effect of Microstructure and Casting Defects on the Mechanical Properties of Secondary AlSi10MnMg(Fe) Test Parts Manufactured by Vacuum Assisted High Pressure Die Casting Technology*; Elsevier Ltd.: Amsterdam, The Netherlands, 2015; Volume 2.
12. Niklas, A.; Orden, S.; Bakedano, A.; Da Silva, M.; Nogués, E.; Fernández-Calvo, A. Effect of solution heat treatment on gas porosity and mechanical properties in a die cast step test part manufactured with a new AlSi10MnMg(Fe) secondary alloy. *Mater. Sci. Eng. A* **2016**, *667*, 376–382. [[CrossRef](#)]
13. Ahn, C.; Lee, E. [ICACE2019] Effect of cooling rate on the corrosion resistance and mechanical property of AlSi10MnMg alloy. *J. Korean Soc. Mar. Eng.* **2019**, *43*, 618–624. [[CrossRef](#)]
14. Shi, J.; Pries, H.; Stammen, E.; Dilger, K. Chemical pretreatment and adhesive bonding properties of high-pressure die cast aluminum alloy: AlSi10MnMg. *Int. J. Adhes. Adhes.* **2015**, *61*, 112–121. [[CrossRef](#)]
15. Jo, I.; Ahn, C.; Lee, E. High-temperature tensile deformation behavior and failure mechanisms of Al-10Si-Mn-Mg high-pressure die-cast alloy. *J. Korean Soc. Mar. Eng.* **2019**, *43*, 788–792. [[CrossRef](#)]
16. Ji, S.; Watson, D.; Fan, Z.; White, M. Development of a super ductile diecast Al–Mg–Si alloy. *Mater. Sci. Eng. A* **2012**, *556*, 824–833. [[CrossRef](#)]
17. Aballe, A.; Bethencourt, M.; Botana, F.J.; Marcos, M.; Osuna, R. Using EIS to study the electrochemical response of alloy AA5083 in solutions of NaCl. *Werkstoffe und Korrosion* **2001**, *52*, 185–192. [[CrossRef](#)]